AIAA JOURNAL
Vol. 39, No. 12, December 2001

Suppression of Self-Sustained Oscillations in a Supersonic Impinging Jet

R. Elavarasan,* A. Krothapalli,† L.Venkatakrishnan,* and L. Lourenco‡
Florida A&M University and Florida State University, Tallahassee, Florida 32310

A passive control technique was used to suppress the self-sustained oscillations in a supersonic impinging jet. A rigid plate, placed in the ambient region close to the jet exit, was used to interrupt the upstream propagating acoustic waves originating from the impingement region. The effectiveness of this technique was examined using the particle image velocimetry. The results clearly showed that the large-scale coherent vortical structures, which dominated the normal impinging jet, are completely suppressed with the passive control technique. As a result, a significant reduction in induced entrainment velocity was found. A recovery of about 16% of the lift loss on the attached lift plate was achieved when compared to an uncontrolled impinging jet. A reduction of about 11 dB in the near-field overall sound pressure level was observed.

I. Introduction

THE suppression of impingement jet noise is of paramount importance for a successful development of a short takeoff and vertical landing (STOVL) aircraft, such as the Joint Strike Fighter. This paper deals with a passive noise control method for the suppression of discrete sound generated by an ideally expanded supersonic impinging jet. Recent near-field acoustic measurements by Krothapalli et al.[1] showed that the jet impingement increases the overall sound pressure level (OASPL) by approximately 8 dB relative to a corresponding freejet. In addition, the spectrum of the noise generated contains discrete frequency sound that is not normally observed in ideally expanded freejets (Fig. 1). Schlieren flow visualizationpictures show a strong organized acoustic wave pattern with its source being located in the jet impingement region. Associated with the wave pattern are large-scale coherent vortices in the jet shear layer as shown in Fig. 2 (jet exit Mach number $M_j = 1.5$, ideally expanded). These flow and acoustic characteristics are a manifestation of the self-excitation due to a well-known feedback mechanism. The physical mechanism involving the feedback mechanism has been studied in detail by many researchers.[1–5] Briefly, on impingement on the wall, the large vortical structures will generate coherent pressure fluctuations,[6] which result in acoustic waves of significant intensity. These acoustic waves travel through the ambient medium and, on reaching the nozzle exit, excite the shear layer of the jet, leading to the generation of the instability waves, thus closing the feedback loop. While investigating the low-speed edgetone flowfield, which is governed by a similar feedback mechanism, Karamcheti et al.[7] suppressed the tone by placing two plates normal to the centerline of the jet in the ambient flow region. Motivated by this observation, we employed a similar technique for the impinging tone suppression in the present experiment.

The large-scale coherent vortices are the dominant feature of the impinging jet, whereas no such structures are present in a corresponding freejet. These structures, while convecting downstream, induce high entrainment velocity in the near field of the jet. As a result, a low-pressure region exists on the flat lift plate flush mounted with the nozzle exit. The low-pressure region generates a suckdown force whose magnitude can reach up to 60% of the main jet thrust.[1] Also, the high-amplitude tones can cause structural damage through sonic fatigue. In such situations, it is highly desirable to suppress the high-frequency/amplitude tones as well as the formation of large-scale structures in the jet.

In the present study, we attempted to modify the feedback loop by means of a passive control device and thereby affect the large-scale motions in the flow. The suppression of large-scale structures is expected to affect the overall noise spectra and the entrainment characteristics. A small metal plate was placed in the outside path of the feedback loop to interrupt the acoustic waves in the ambient medium reaching the nozzle exit. The effectiveness of such a technique on the flowfield is examined using the particle image velocimetry (PIV) technique, mean surface pressure on the lift plate, and near-field acoustic measurements.

II. Experimental Setup

Experiments were carried out in the STOVL research facility of the Fluid Mechanics Research Laboratory at Florida State University. The facility has been used to study the jet-induced forces on STOVL-configured aircraft models hovering in and out of ground effect. Positioning the ground plane at various heights relative to the model through a traversing mechanism simulated the hovering effect. An aluminum plate of size 1 m × 1 m × 25 mm served as a ground plane. The height between the ground plane and nozzle exit h was varied from 0.04 to 1.5 m. The schematic of the experimental setup is shown in Fig. 3a. A shock-free nearly ideally expanded jet was obtained from a converging–diverging (C–D) axisymmetric nozzle. The throat and exit diameters are 2.54 and 2.75 cm, respectively. The nozzle was designed for an exit Mach number of 1.5. The divergent portion of the nozzle was a straight conic section with a 3-deg divergence angle.

To simulate the airframe of the STOVL aircraft, a circular lift plate is used. From a detailed investigation using several size lift plates, it was found that a ratio between the nozzle exit diameter and the lift plate diameter of 1:10 is adequate for a meaningful estimation of the lift force. A circular lift plate of diameter 25.4 cm d was flush mounted with the nozzle. The circular plate contained 17 pressure taps arranged along a radial line, and the pressure was measured with a Validyne™ strain gauge transducer mounted in a Scanivalve™ unit. At each port, several seconds of digitized data were taken. The force on the lift plate was calculated from the jet-induced mean surface pressures.

The near-field acoustic measurements were made using a 0.635-cm-diam B&K microphone placed at 25 cm away from the nozzle exit and at 90 deg to the jet axis. The microphone signal and the lift plate surface pressures were acquired through a National Instruments data acquisition system with associated Lab View™ software.

Received 10 April 2000; revision received 5 May 2001; accepted for publication 14 May 2001.

*Research Associate, Department of Mechanical Engineering, 2525 Pottsdamer Street.

†Don Fuqua Eminent Scholar and Chairman, Department of Mechanical Engineering, 2525 Pottsdamer Street. Associate Fellow AIAA.

‡Professor, Department of Mechanical Engineering, 2525 Pottsdamer Street. Member AIAA.

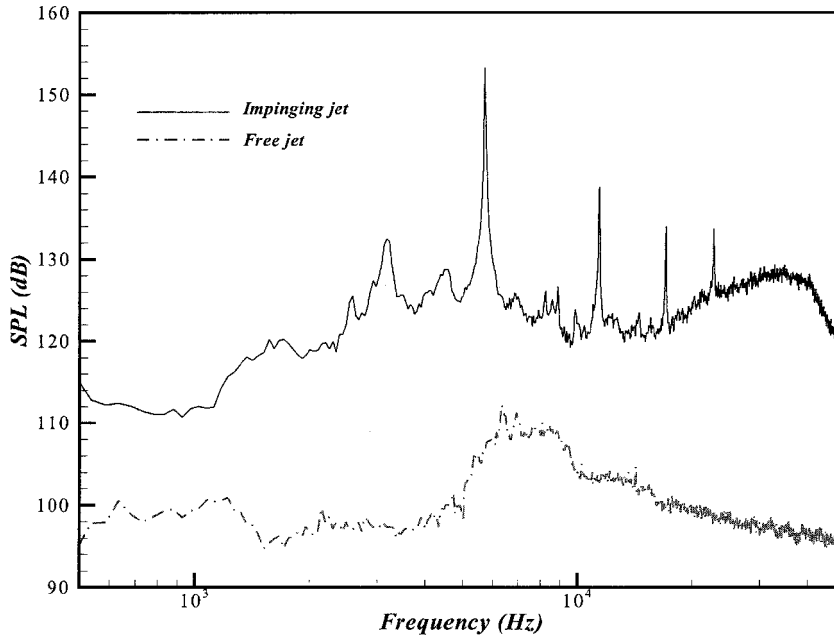

Fig. 1 Near-field narrow band noise spectra of ideally expanded freejet and impinging jet: $M_j = 1.5$, jet throat diameter $D = 27.5$ mm, for impinging jet $h/D = 4$ (microphone location, $10D$ from jet centerline).

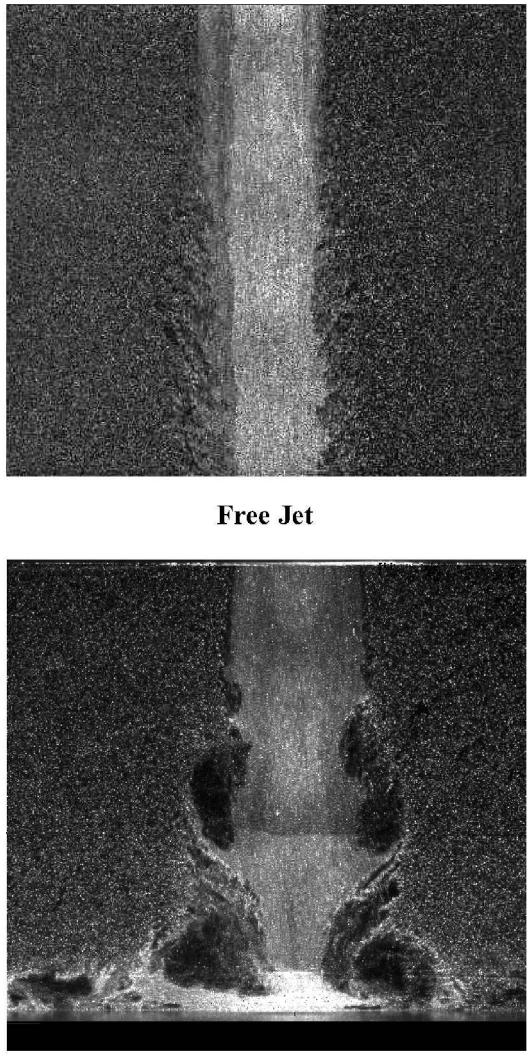

Fig. 2 Instantaneous PIV images of free and impinging supersonic jets: $M_j = 1.5$.

For the acoustic measurements, the nearby exposed metal surfaces were covered with 10-cm-thick acoustic foam to minimize sound reflections.

The control plate used to interrupt the acoustic waves was made of 2.5-mm-thick aluminum plate and mounted close to the nozzle exit as shown in Fig. 3b. Experiments were conducted with two control plates of different geometries: a simple rectangular plate of size 89×26 mm, a rectangular plate (89×76 mm) with a semicircular cut. From the experimental data, it was found that the control plate with semicircular cut proved to be more effective in suppressing the unsteady oscillation and large-scale structures. Hence, most of the results presented here were obtained with the semicircle control plate. The control plate was placed 7 mm downstream of the nozzle exit and 1.6 mm away from the nozzle lip. It was supported by a support device, which held the control plate in its location firmly. The optimum location of the control plate with respect to the jet exit shown in Fig. 3 was found to be most effective in suppressing the large-scale oscillations of the jet. At no time does the control plate interfere with the jet. All of the experiments were conducted at a nozzle exit Mach number of 1.5 and a fixed normalized ground plane height of $\boldsymbol{h/D} = 4$, where $\boldsymbol{D}$ is the nozzle throat diameter. The choice of the operating pressure and ground plane height was decided based on the earlier experiments[1] conducted in the same facility. Because the main purpose of the present study is to suppress the unsteady oscillations of the jet by affecting the feedback loop, it was decided to carry out the experiments at a condition where the largest amplitude of the impinging tone was observed.

A top hat velocity profile with laminar boundary layers was maintained at the nozzle exit. The jet stagnation temperature was maintained to within $\pm 2^\circ$ of 20°C. The nominal exit Reynolds number, based on the nozzle exit diameter and the exit velocity was 7×10^5. A cylindrical coordinate system is used with its $\boldsymbol{x}$ axis aligned with the centerline of the jet, and $\boldsymbol{r}$ represents the radial direction. The corresponding velocity components are $\boldsymbol{u}$ and $\boldsymbol{v}$, respectively.

III. PIV

PIV is being used to measure the instantaneous velocity field in a selected plane of the flowfield. With novel image processing algorithms, it is possible to measure supersonic jet flows with fidelity.[1,8] In the present experiment, a double-pulsed Nd:YAG laser (Spectra-Physics-PIV400; 400 mJ) was used to produce a light sheet of about 1-mm thickness (Fig. 3a). A charge-coupled device camera (Kodak ES1.0) was used to capture the particle images. The resolution of the camera was 1×1 K and operated in double-exposure mode. In this

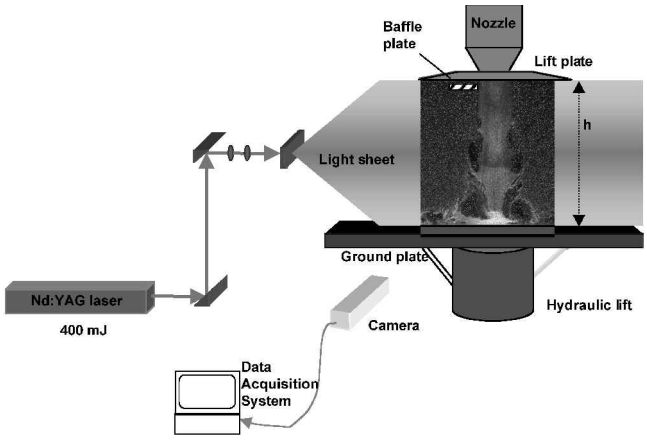

Fig. 3a PIV experimental setup.

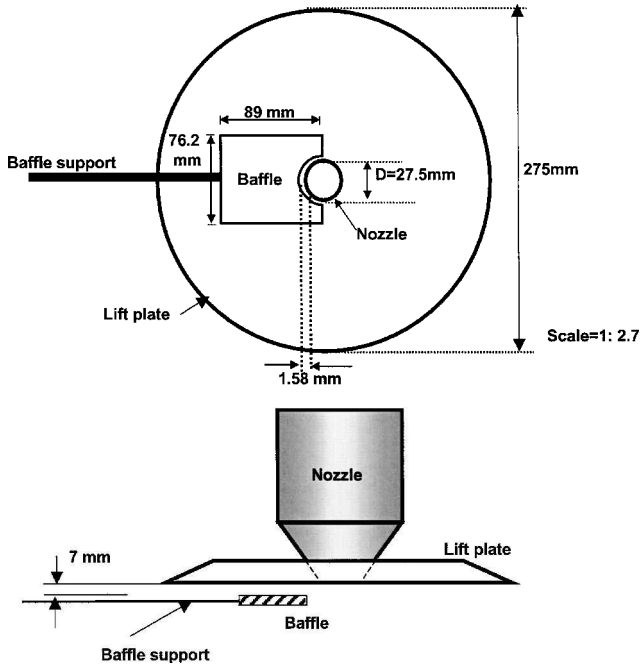

Fig. 3b Control plate geometry and location with respect to nozzle.

mode of operation, with proper synchronization with laser pulses, the camera can acquire 15 image pairs per second. The images are transferred to a computer through an Imaging Technologies ICPCI board. An in-house developed cross correlation algorithm was used to extract the velocity information from the double-exposed images. The algorithm uses a novel mesh-free approach with high spatial resolution and identifies each particle image pair and associated position.[9] At each experimental condition, 160 pairs of instantaneous image pairs were obtained. The maximum area imaged in the present experiment was 120×120 mm, and the time interval between pulses was 1.7 s. The images were analyzed using a rectangular grid of 80×80 interrogation cells with an interrogation cell of size 8×8 pixels.

In the PIV experiments, the velocity is obtained by measuring the displacement of the seeded particles in the flow at two successive times. Hence, it is important to choose proper seeding particles that follow the fluid motion accurately. In supersonic flows the particles encounter considerable acceleration and deceleration. In addition, because of variations in flow density, the seeding particle density also varies, with the highest particle density being in the low-speed regions. The situation becomes more severe when the shocks are present in the flow. A detailed study by Ross[10] provided a useful guideline to choose proper seeding particles for supersonic flows. The results indicated that the particle relaxation length varies significantly with the shock strength and the particle diameter. The relaxation length is a function of the shock strength parameter ($\Delta p/p$) and exit temperature. For a 1-μm particle in a flow with shock strength parameter $\Delta p/p = 0.37$ and an exit temperature of 60°F, the relaxation length is about 6.5 mm. In the present experiment, the compression in the flow results in much smaller values of the shock strength parameter, and, as a result, the relaxation lengths are expected to be much smaller. In the present experiment the jet was seeded with oil droplets ($\sim$1 μm; Rosco fog fluid) generated by a Wright nebulizer (a device consisting of multiple atomizers and driven by high-pressure air). The flow rate of the seeding particles was controlled in such a way that there were enough particles in the jet. The ambient air was seeded with smoke particles ($\sim$2 μm) produced by a commercial fog generator (Rosco). Because the jet was operated at an ideally expanded condition, there were no shock cells present in the flow. At this condition the velocity of the particles was found to be in close agreement ($\pm$2%) with the calculated exit velocity using isentropic relations.

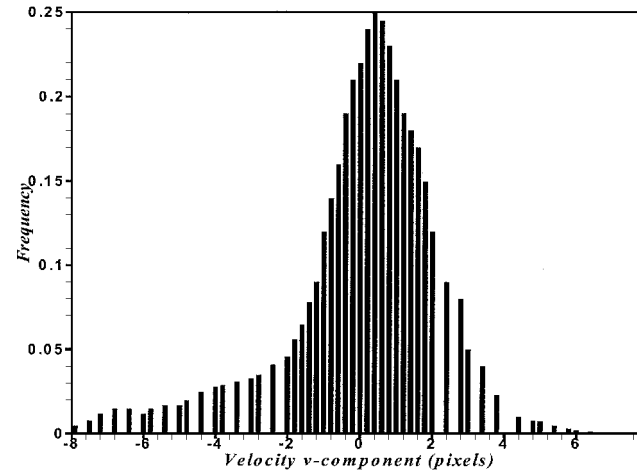

Fig. 4 Histogram of radial velocity distribution of an impinging jet (Fig. 2b).

Figure 4 shows a histogram of the radial velocity distribution of an impinging jet from Fig. 2b.

IV. Validation of PIV Measurements

The accuracy of the PIV technique depends on many parameters, such as selection of seeding particles and their response to sudden changes in flow condition and the processing algorithm. The details of the selection of the seeding particles and their response to sudden changes in the flow conditions have already been discussed. Apart from the selection of the seeding particle, the important aspect that decides the accuracy of the PIV measurement is the methodology used in processing the PIV images. The details of the processing scheme used in the present PIV measurements can be found in Ref. 11.

To verify the accuracy of the PIV technique in the supersonic flow, the result (reproduced from Alkislar[12]) of an underexpanded rectangular jet ($M_j = 1.69$) is shown in Fig. 5a. The design Mach number of the nozzle is 1.44. The x and y coordinates were aligned with the lateral and transverse directions, respectively. The height of the nozzle is 10 mm. The expansion of the jet and formation of the shock cells are very clearly captured by PIV. The expansion angle of the jet near the nozzle was calculated theoretically using a Prandtl–Meyer function and was found to be 7.37 deg. The angle measured in the present experiment is 7.25 deg, with a difference of less than 1% when compared to theoretical calculation. In Fig. 5b, the distribution of centerline velocity is shown and compared with pressure probe data. The pressure data combined with static temperature data reveal the velocity by using the isentropic relations in the inviscid portion of the jet. As can be seen, a very good agreement between the two data with a maximum error of about 2% is observed. Near the nozzle exit, the measured velocity with PIV is 442 m/s, whereas the theoretical calculation provided a value of 445 m/s, with a relative discrepancy of about 0.7%. These observations support the finding that the selection of seeding particles and the usage of the

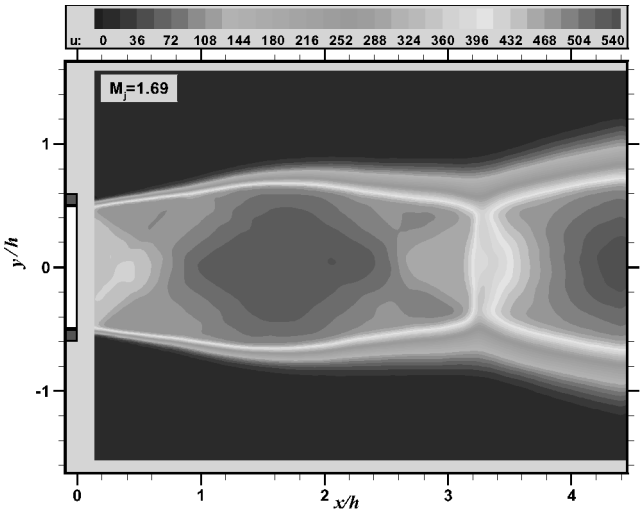

Fig. 5a Mean U velocity field of an underexpanded jet: $M_j = 1.69$.

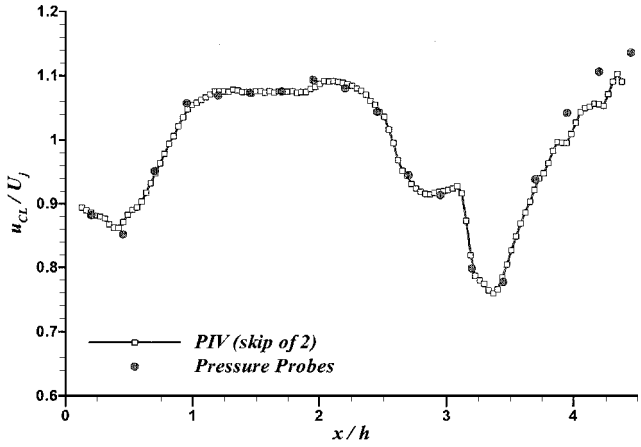

Fig. 5b Comparison of centerline velocity measured by PIV and pressure probe.

appropriate algorithm yield accurate results in a supersonic shear flow.

V. Results and Discussion

The PIV technique has a distinct advantage of providing good quality flow images that can be used for flow visualization purposes. Figures 6a and 6b show typical double-exposed particle images of impinging jets ($h/D = 4$) for two different control plates (the simple rectangular plate and plate with semicircle cut). It was shown earlier that, at this particular height, the uncontrolled impinging jet (Fig. 2b) is dominated by large-scale structures. With the introduction of the control plates, the formation of these structures appears to be affected significantly, which can be clearly seen in Figs. 6a, and 6b. However, the semicircle control plate (Fig. 6b) appears to be more effective in eliminating large-scale structures. In anticipation of a better control, a full circular control plate was also used. However, the large organized structures reappeared in the jet. This is due to the control plate acting like a small lift plate, thereby reinforcing the feedback loop. The strong coupling between the sound waves and the instability waves takes place over the distance of a few instability wavelengths immediately downstream of the nozzle exit. Because the downstream location of the full circular control plate is within this region, the feedback loop reestablished itself, giving rise to self-sustained oscillations of the jet. The sound produced at the impingement region and the resulting upstream propagating acoustic modes are found to be axisymmetric in nature.[1] The control plates used here simply interrupt the upstream propagating acoustic waves from reaching the nozzle exit region. In addition, they also weaken the coherence of the axisymmetric acoustic mode that is responsible for the excitation of the shear layer instability waves at the nozzle exit. The extent of modification of the complex interaction process at the nozzle exit depends on the geometry of the control plate used.

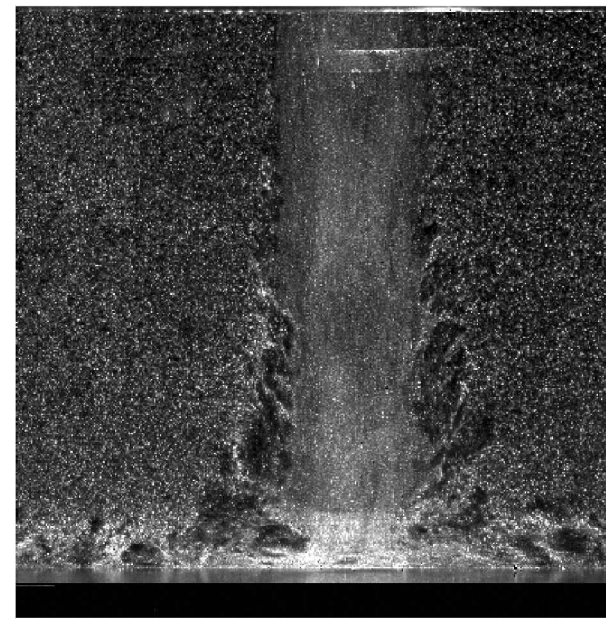

a) With rectangular control plate

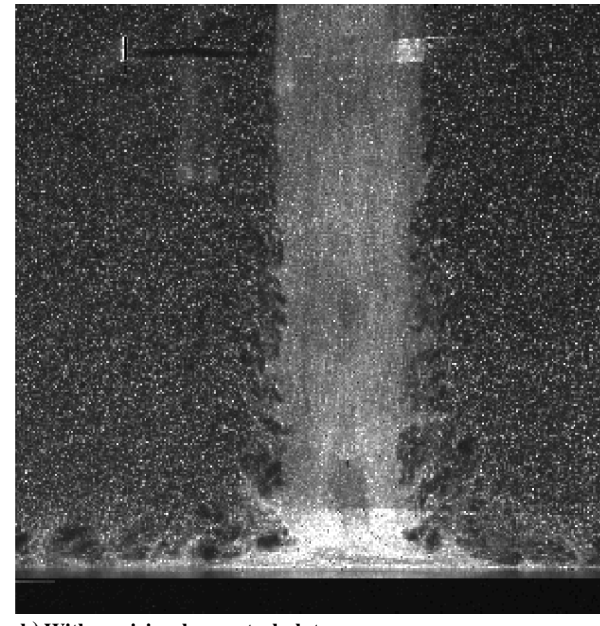

b) With semicircular control plate

Fig. 6 Instantaneous PIV images of impinging jet at $h/D = 4$ with control plates.

The instantaneous velocity fields superimposed with the out-of-plane component of vorticity, corresponding to the particle images (Figs. 2b and 6b) are shown in Fig. 7. In the controlled jet experiments (Fig. 7b), the presence of the semicircular control plate resulted in the lack of velocity measurements within the first 20 mm of the nozzle exit. However, the conclusions reached in the present experiment were not affected by this lack of information near the nozzle exit. Figure 7 clearly shows the details of different regions of the flow consisting of the impingement region and the wall jet. The large-scale motions in the uncontrolled impinging jet are clearly captured by the PIV measurement. Unlike in Fig. 7a, the shear layer in the case with the control plate appears to be free of any large-scale vortical regions. The instantaneous centerline variation of the axial component of the velocity extracted from Figs. 7a and

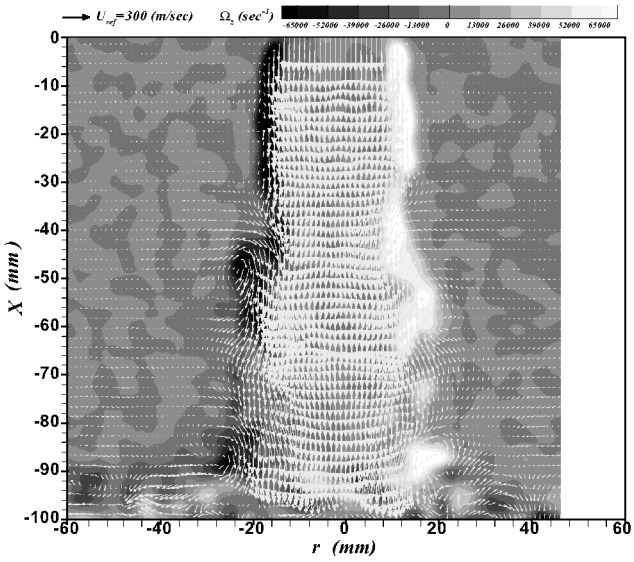

a) No control plate

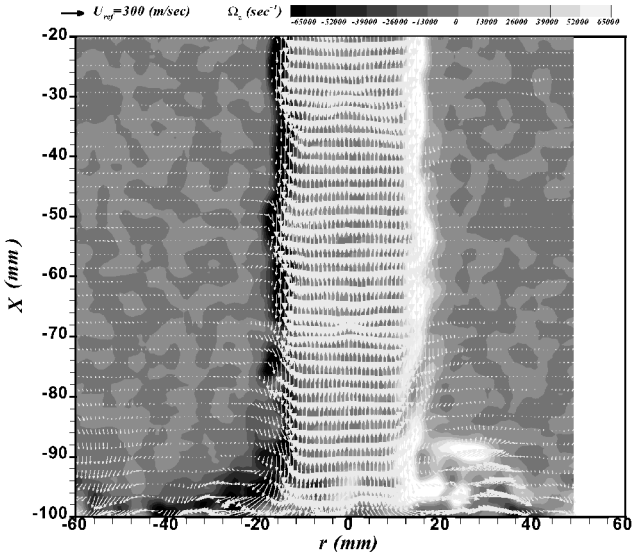

b) With semicircular control plate

Fig. 7 Instantaneous velocity fields corresponding to impinging jet at $h/D = 4$.

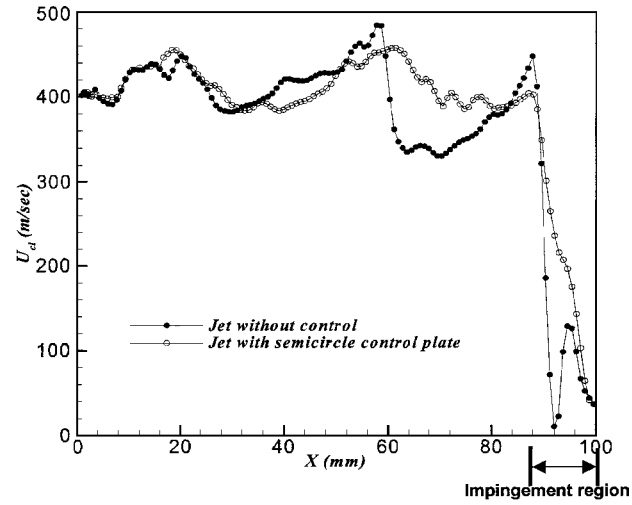

Fig. 8 Centerline velocity variation along jet with and without control plate.

7b is shown in Fig. 8. The centerline axial velocity variation for both cases is nearly the same, suggesting that the changes brought out by the passive control plate are mostly confined to the shear layer.

A traditional but useful way of examining the organized motions is through the calculation of a space–time velocity correlation function.[13,14] The regions of correlated velocity are used to identify the large-scale coherent structures in the flow. The whole field PIV data lend themselves to easy determination of the spatially correlated regions of the flow. In the present study, the correlation is used to show the elimination of the large structures in the shear layer after introduction of the passive control technique. The high values of the correlation function $\boldsymbol{R}_{ij}$ (i and j correspond to the $\boldsymbol{u}$ and $\boldsymbol{v}$ velocity components, respectively), as defined hereafter, indicate the presence of a spatially coherent region.

For a statistically steady flow, the space–time correlation function of axial component of the velocity R_{uu} can be written as

$$R_{uu}(\Delta x, r, \Delta t) = \frac{u(x, r, t)u(x + \Delta x, r, t + \Delta t)}{u_{\text{rms}}(x)u_{\text{rms}}(r)} \qquad (1)$$

where Δt is the time delay and $\boldsymbol{u}$ is the axial component of velocity. In the present study, the correlation function was calculated with zero time delay, and Eq. (1) for the correlation of turbulent axial velocity reduces to

$$R_{uu}(x, x_r) = \frac{\overline{u'(x)}\,\overline{u'(x_r)}}{u'_{\text{rms}}(x)u'_{\text{rms}}(x_r)} \qquad (2)$$

where $\boldsymbol{x}_r$ is the reference location in the flow and u' is the fluctuating component obtained by subtracting the mean velocity field from each instantaneous velocity field. The reference location was varied along the center of the shear layer in steps of jet diameter and correlated with all points in the fluctuating velocity field. This was averaged over 160 fields.

The resultant isocontours of spatial correlation function are plotted in Figs. 9a and 9b, corresponding to the uncontrolled (Fig. 2b) and controlled jets (Fig. 6b), respectively. In the uncontrolled jet, the well-correlated region ($R_{uu} \geq 0.8$) can be seen extending symmetrically around the jet, confirming the presence of large-scale coherent structure in that region. The extent of the correlation contours approximately indicates the size of the structure. The result agrees very well with the visual observation and velocity measurements. In the controlled jet case (Fig. 9b), note that the correlated regions are confined to a much smaller area, indicating the absence of large-scale structures.

The magnitude of the surface pressures on the lift plate is closely linked to the jet entrainment velocities induced by the large structures in the shear layer, especially when the jet is confined by two solid boundaries (lift plate and the ground plane). To observe the induced velocity field, the corresponding regions of the velocity field containing the large-scale structure in Figs. 7a and 7b are enlarged in Figs. 10a and 10b, respectively. Also included in Fig. 10 are the streak lines introduced at selected locations in the entrainment region. The fluid in the vicinity of the vorticity-bearing fluid is set in motion through the Biot–Savart induced velocity field. Irrotational fluid sufficiently close to the vortical fluid will, in fact, participate in the large-scale structure motions as shown in Fig. 8a. In the absence of large-scale structures (Fig. 10b) the induced entrainment velocity magnitude is lower compared to the uncontrolled case. In general, the entrainment velocity represents the radial influx of the ambient fluid into the main jet and is measured along the shear layer. In the present experiment, the entrainment characteristics were studied by estimating the actual velocity magnitude $[\boldsymbol{q} = (\boldsymbol{u}^2 + \boldsymbol{v}^2)^{1/2}]$ measured in the near hydrodynamic field. Note that the main contribution for the velocity magnitude is derived from a radial component of the velocity. Though the entrainment velocity and velocity magnitude are defined in a different fashion, both of them refer to the induced flowfield around the jet. Because there is no proper definition for defining the near hydrodynamics field, a distance of one diameter from the jet shear layer is generally considered to be near

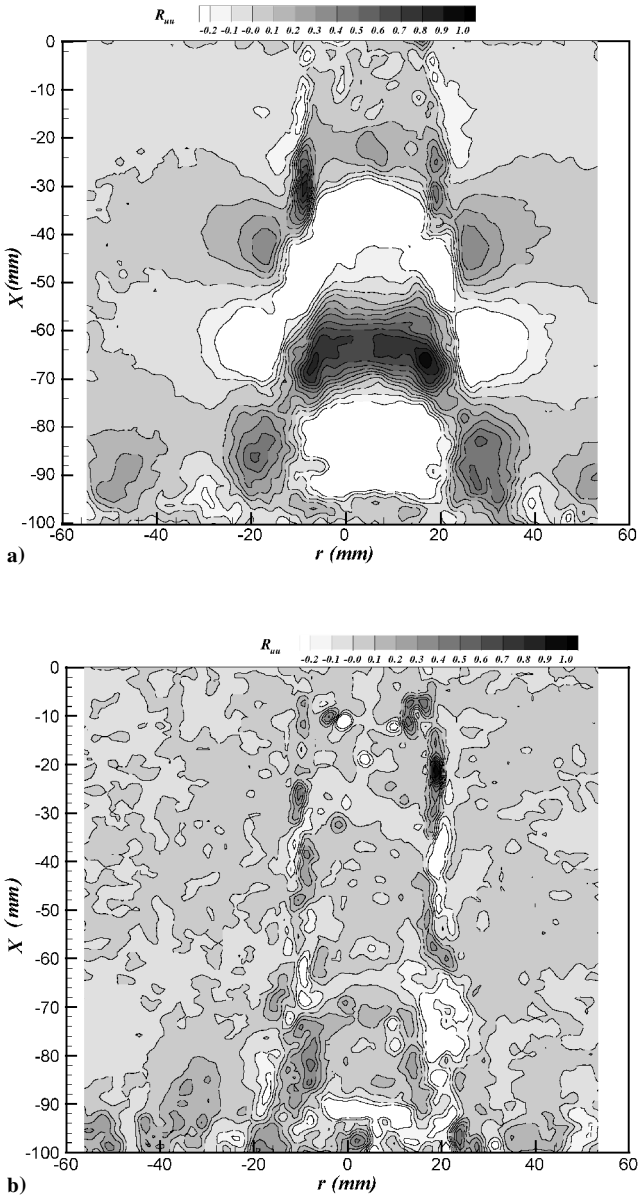

Fig. 9 Isocontours of correlation function R_{uu}: a) uncontrolled jet, contours show presence of large-scale structures and b) with semicircular control plate.

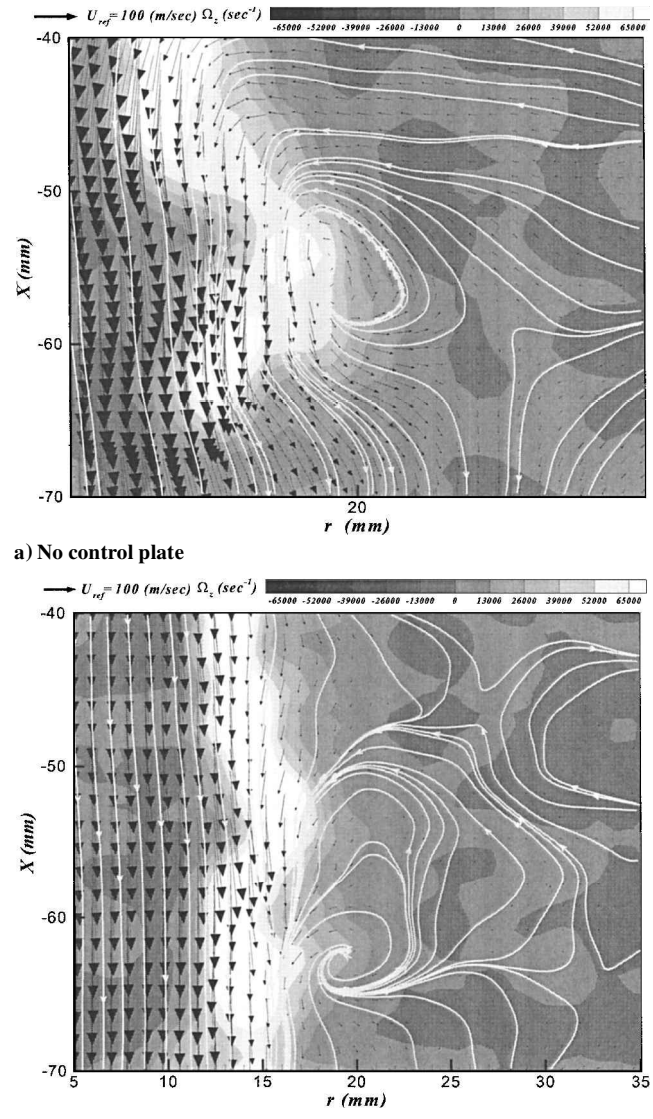

Fig. 10 Enlarged view of jet shear layer shows effect of control plate on large-scale motions; streak lines indicate induced flow in near hydrodynamics field.

field. For consistency, the velocity magnitude was measured at 1.5*d* from the jet centerline. Typical variation of velocity magnitude with downstream distance is shown in Fig. 11. The velocity magnitude for a freejet is also plotted for comparison. The magnitude of the near-field instantaneous entrainment velocity for the uncontrolled impinging jet can reach up to 80 m/s as shown in Fig. 11. The peak entrainment velocities seem to occur at the locations where large-scale structures are located in Fig. 2b. In the presence of the control plates, the magnitude of the entrainment velocity has reduced significantly when compared to the uncontrolled jet. In this case, the magnitude of the velocity is about 10 m/s, quite similar to that observed for a freejet.[1] The high entrainment velocities induced in the near hydrodynamic field by the large-scale structures will result in relatively high suction pressures on the bottom surface of the lift plate for the case without the control plate.

To assess the amount of negative lift force produced on the lift plate, the mean surface pressure measurements on the lift plate were carried out. Figure 12 shows the surface pressure distribution over the lift plate with and without a control plate. Because the measurements indicated that the pressure distribution was symmetric on the lift plate, only the results obtained on one side of the plate are shown here. Figure 12 shows that for the controlled jet, except near

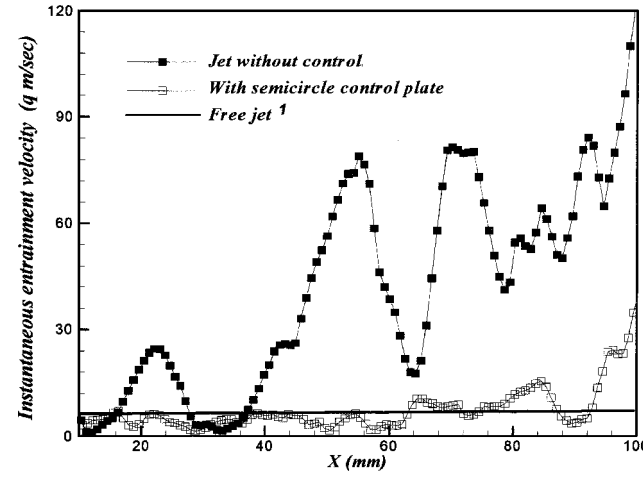

Fig. 11 Instantaneous entrainment velocities measured at $r/D = 1.5$ from jet centerline.

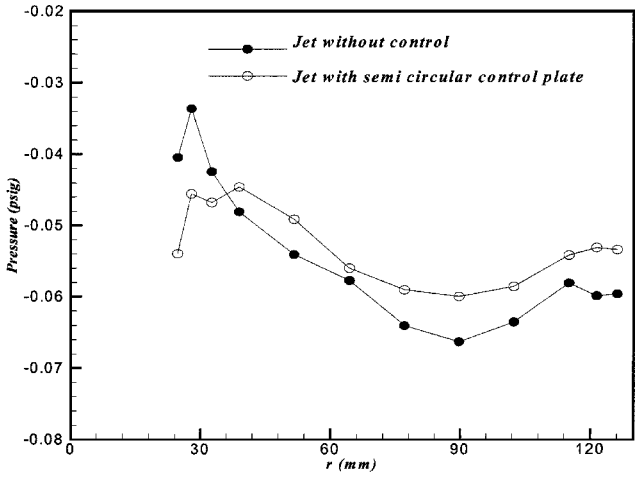

Fig. 12 Mean pressure distribution on lift plate.

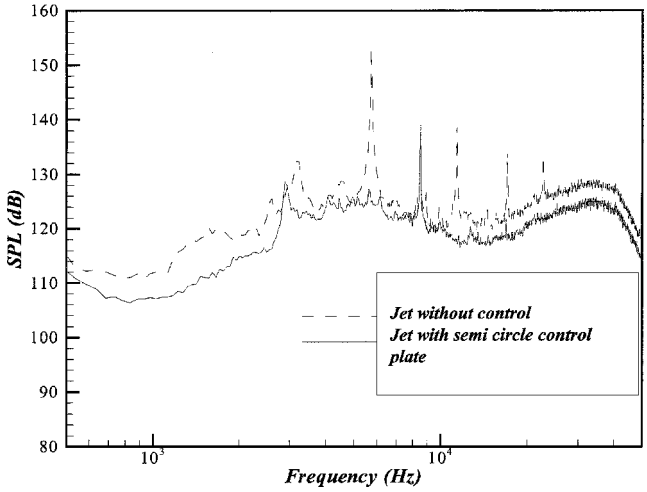

Fig. 13 Near-field narrow band spectra with and without control plate.

the nozzle exit, the mean pressure is higher than the uncontrolled jet. This indicates that there is a drop in suckdown force on the lift plate as a result of the control device. For estimating the net lift loss, the lift force is obtained by integrating the pressure distribution (Fig. 12) over the entire area of the lift plate. This is normalized with the jet thrust, which was calculated using one-dimensional isentropic relations. The results indicate a decrease in the downward force of about 16% with a control device as compared to that of the uncontrolled impinging jet. The pressure distribution on the control plate was not measured; as a result, it was not taken into account in the force estimation. However, its contribution to the total force may be relatively small. The results just discussed clearly show that the passive control technique has a positive influence on the lift loss recovery.

The effect of the control plate on the acoustic characteristics is described through the near-field microphone measurements. Figure 13 shows the typical near-field narrow band noise spectra for an uncontrolled and a controlled impinging jet. A broad peak corresponding to the broadband shock associated noise (generated due to the presence of weak shock cell structure) is present in both cases. In the uncontrolled jet case, prominent discrete tones, commonly called impinging tones, are present with a prominent tone at 5875 Hz. These tones are a manifestation of the impingement process and the magnitude of this tone can be seen reaching up to 155 dB. This observation agrees well with the measurement of Krothapalli et al.[1] The other smaller peaks in the spectrum are associated with the harmonics of the impinging tones.

Significant changes can be observed in the controlled jet noise spectrum. One of the prominent differences as compared to the uncontrolled jet spectrum is the reduction of the broadband noise over the entire range of the spectrum. The other important change is the complete suppression of the impinging tone (5875 Hz). However, another peak with lower amplitude (15 dB lower than the impinging tone) appears at the higher frequency (8000 Hz) side of the spectrum. Apart from this tone, there are no other noticeable tones. It is speculated that the high-frequency tone that appear in the control jet case might be a result of interaction of the acoustic waves with the sharp edges of the control plate.

To assess the overall all noise reduction in the controlled jet cases the OASPL are calculated. The OASPL values are found to be 159 and 148 dB for uncontrolled and controlled jets, respectively. The results indicate that a considerable (about 11 dB) reduction in the overall noise level can be achieved by the passive control technique, in addition to the suppression of self-sustained oscillation resulting from the feedback mechanism.

VI. Conclusions

A simple passive control technique has been successfully used to modify the acoustic feedback mechanism in a supersonic impinging jet. This technique involves placing a control plate close to the nozzle exit so that the upstream propagating acoustic waves can be blocked from reaching the jet exit. PIV, pressure, and microphone measurements were carried out to study the flow behavior and assess the modifications brought out by the control plate. The control plate appears to weaken the feedback loop and prevent the onset of self-sustained oscillations in the jet. This resulted in the suppression of large-scale motions, which are believed to be the root cause for the generation of suckdown forces and to be a prominent source of noise. On testing various control plate geometries, it was found that a control plate with a semicircle cut, which covers 50% of the nozzle exit, proved to be more effective. A recovery of about 16% lift loss was achieved with this configuration. The suppression of large-scale structures in the flow also resulted in a reduction of 11dB in OASPL. The results shown in the paper clearly demonstrate that the interruption of the feedback loop yields significant reductions in the lift loss and the near-field noise levels. A practical implementation of the technique on an airplane can be done by deploying a rigid plate (similar to a flap) from the belly of the aircraft at the nozzle exit.

Acknowledgments

The authors thank the continued support of NASA Ames Research Center through a grant monitored by Douglas Wardwell. We would like to thank the reviewers and the associate editor for their helpful comments. We would also like to thank Bahadir Alkislar for providing us the particle image velocity data to demonstrate the accuracy of the technique.

References

[1] Krothapalli, A., Rajakuperan, E., Alvi, F., and Lourenco, L., "Flow Field and Noise Characteristics of a Supersonic Impinging Jet," *Journal of Fluid Mechanics*, Vol. 392, 1999, pp. 155–181.

[2] Powell, A., "On the Mechanism of Choked Jet Noise," *Proceedings of the Physical Society, London, Section B*, Vol. 66, 1953, pp. 1039–1057.

[3] Powell, A., "The Sound-Producing Oscillations of Round Underexpanded Jets Impinging on Normal Plates," *Journal of the Acoustical Society of America*, Vol. 83, No. 2, 1988, pp. 515–533.

[4] Neuwerth, G., "Acoustic Feedback of a Subsonic and Supersonic Free Jet Which Impinges on an Obstacle," NASA TT F-15719, 1974.

[5] Tam, C. K. W., and Ahuja, K. K., "Theoretical Model of Discrete Tone Generation by Impinging Jets," *Journal of Fluid Mechanics*, Vol. 214, 1990, pp. 67–87.

[6] Alvi, F. S., and Iyer, K. G., "Mean and Unsteady Flowfield Properties of Supersonic Impinging Jets with Lift Plates," AIAA Paper 99-1829, May 1999.

[7] Karamcheti, K., Bauer, A. B., Shields, W. L., Stegen, G. R., and Woolley, J. P., "Some Features of an Edge Tone Flow Field," NASA SP-207, 1969, pp. 275–304.

[8] Elavarasan, R., Lourenco, L., Venkatakrishnan, L., and Krothapalli, A., "Application of PIV to Large-Scale STOVL Supersonic Jet Facility," AIAA Paper 99-0271, Jan. 1999.

[9]Lourenco, L.M., and Krothapalli, A., "Mesh-Free, Second-Order Accurate Algorithm for PIV Processing," *Proceedings of International Conference on Optical Technology and Image Processing in Fluid, Thermal and Combustion Flow*, Yokohama, Japan, 1998.

[10]Ross, C. B., "Calibration of Particle Image Velocimetry in a Shock-Containing Supersonic Flow," M.S. Thesis, Dept. of Mechanical Engineering, Florida State Univ., Tallahassee, FL, May 1993.

[11]Lourenco, L., and Krothapalli, A., "True Resolution PIV: A Mesh-Free Second-Order Accurate Algorithm," *Proceedings of the 10th International Symposium on Applications of Laser Techniques in Fluid Mechanics*, Lisbon, 2000.

[12]Alkislar, M. B., "Flow Field Measurements in a Screeching Rectangular Jet," Ph.D. Dissertation, Dept. of Mechanical Engineering, Florida State Univ., Tallahassee, FL, Aug. 2001.

[13]Dumas, R., "Observations on the Boundary Layer Based on Measured Correlations with Various Improvements," *Near-Wall Turbulence*, edited by S. J. Kline and N. H. Afgan, Hemisphere, New York, 1991, pp, 437–452.

[14]Kim, J., and Hussain, F., "Propagation Velocity and Space–Time Correlation of Perturbations in Turbulent Channel Flow," NASA TM-103932, 1992.

J. C. Hermanson
Associate Editor